

Solid-State Conformational Isomerism Lacking a Gas-Phase Energy Barrier: Its Structural, Spectroscopic, and Theoretical Identification in an Organochromium(III) Complex

Helge-Boj Hansen, J. Krzystek, Joshua Telser,* Abinash Swain, Gopalan Rajaraman, Hubert Wadepohl, and Markus Enders*



Cite This: *Organometallics* 2022, 41, 1558–1564



Read Online

ACCESS |



Metrics & More

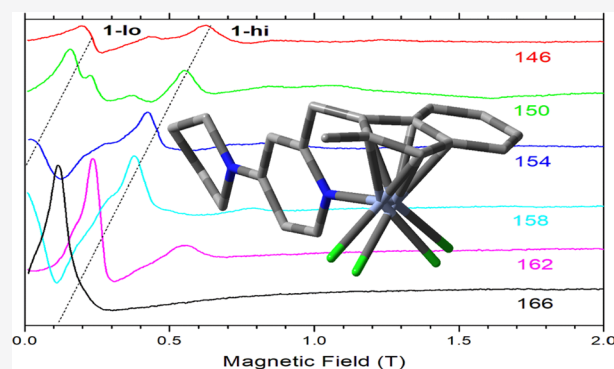


Article Recommendations



Supporting Information

ABSTRACT: We present a combined X-ray diffraction (XRD), high-frequency and -field electron paramagnetic resonance (HF-EPR), and theoretical study of an organochromium(III) complex with relevance to polymerization catalysis that crystallizes in a disordered structure with two conformational isomers in a ratio of 0.89:0.11. The structure is exceptional, as the disorder is restricted to the CrCl_2 moiety, whereas the organic ligand is not disordered within the precision of the structure determination. Although the geometry is only slightly varied, these Cr(III) ($3d^3$, $S = 3/2$) isomers give substantially different EPR spectra so that both species can be analyzed in terms of distinct zero-field splitting (zfs) parameters. Using the solid-state molecular structure of each isomer, calculated spin Hamiltonian parameters using high-level *ab initio* methods are in good accordance with the experimental results. However, no energy barrier could be identified by calculation of the gas-phase molecular structure, leading to the conclusion that the occurrence of the two isomers is due to intermolecular interactions in the solid state. These results highlight the subtle structural differences that can exist in organometallic complexes. Such structural conformations might well be accessible in solutions of precatalysts and active polymerization catalysts affecting their reactivity.



INTRODUCTION

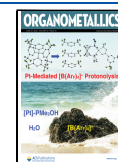
It is a quite common occurrence that two or more conformers are present in single crystals of a given compound. They represent minima on the potential energy surface with a defined barrier for their interconversion. In a crystal, such conformers might be frozen so that the individual structures can be established by X-ray diffraction (XRD). On the other hand, vibrational modes may exist in the solid state, which leads to a dynamic disorder. Such cases are quite common and prevent a precise localization of atomic positions from XRD. However, at low temperatures, a dynamic disorder of larger moieties is unlikely. These two or more structures found in the solid state by XRD can be modeled by theoretical methods, which allows the determination of the energy of these conformers and of their transition state. However, it may happen that in a gas-phase calculation, no energy barrier separates the conformers found in the solid state so that an intermediate structure results.

A property that is very sensitive to small changes in the molecular structure of $S > 1/2$ paramagnetic complexes is zero-field splitting (zfs).^{1,2} Electron paramagnetic resonance (EPR) spectroscopy, particularly in its high-frequency and -field configuration (HF-EPR), is a valuable tool for the precise determination of zfs parameters.³ In parallel with this

experimental tool, state-of-the-art quantum chemical theory (QCT) methods allow the calculation of spin Hamiltonian parameters, including the zfs and g -tensors. In addition, the calculation of the total energies of different geometries provides insight into the gas-phase potential energy landscape with local minima and energy barriers for the interconversion of conformational isomers. Of particular relevance to organometallic chemistry, the appearance of conformational isomers is a well-known phenomenon, especially in indenyl-based metal complexes where ring slippage may have considerable influence on the catalytic properties of metal complexes.^{4,5} Ring slippage is typically observed in the solid state by XRD and in solution by ^1H and ^{13}C NMR of diamagnetic organometallic complexes. Paramagnetic organometallic complexes are less commonly encountered, and how EPR could be used to observe this phenomenon is less clear. Here, we demonstrate that HF-EPR

Received: April 11, 2022

Published: June 9, 2022



can be applied to an $S = 3/2$ organochromium(III) and allow observation of a type of ring slippage in the solid state that is not visible in solution.

RESULTS

We have recently reported the synthesis and catalytic performance of a series of organochromium complexes of type A (Figure 1) where cyclopentadienyl or indenyl ligands

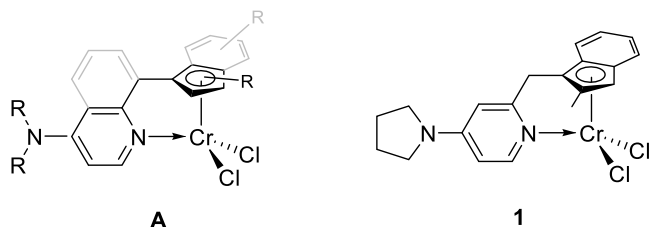


Figure 1. General constitution of complexes of type A reported earlier (left) and the new derivative **1** (right). For the synthetic procedure and analytical data, see the [Experimental Section](#).

were combined with pyridines or quinolines, which themselves carry an electron-donating amino group. These complexes, after activation with methylaluminumoxane, serve as highly active catalysts for the formation of ultrahigh-molecular-weight polyethylene (UHMW-PE).⁶ The solid-state molecular structures of 12 derivatives of **A** were determined by XRD and showed the expected geometries.⁷ Here, we report the synthesis, structural, and electronic properties of a new member of this series, complex **1** (Figure 1), which exhibits properties that are peculiar in comparison to the derivatives reported earlier.

The constitution of **1** is derived from elemental analysis and mass spectrometry, as well as paramagnetic NMR spectroscopy, which showed only one species in CD_2Cl_2 solution (see the [Experimental Section](#)).

XRD. Slow diffusion of *n*-pentane into a solution of complex **1** in dichloromethane led to the formation of crystals suitable for XRD. At first sight, the structure obtained from data collected at 120 K was in accordance with the expected structural type A. However, additional electron density could be explained with a refined model consisting of a superposition of two structural isomers **1a** and **1b** (see details in the [SI](#)). The two structures differ by the position of the chromium center and the corresponding chlorine atoms with respect to the chelating κ^1 -pyridyl- η^5 -indenyl ligand (Figure 2 and Table 1). No disorder was detected in the relevant (coordinating) part of

Table 1. Relevant Metrics for **1a** and **1b** from XRD (Distances in Å and Angles in Degrees); See [Figure 2](#) for Numbering

| metric | 1a | 1b |
|--|---|---|
| Cr-N1 (pyridyl) | 2.078(2) | 2.097(5) |
| Cr-Cl1, Cr-Cl2, avg | 2.2883(9), 2.2933(10), 2.291 | 2.318(8), 2.230(8), 2.274 |
| Cr-Cp | | |
| distance to centroid | 1.888(1) | 1.973(6) |
| distance to mean plane | 1.8858(11) | 1.966(7) |
| Cr-C8, Cr-C9, Cr-C10 Cr-C11, Cr-C12 Cr-C11/C12 (avg) | 2.157(2), 2.215(3), 2.236(3) 2.341(2), 2.270(2) 2.306 | 2.310(6), 2.534(6), 2.390(6) 2.206(5), 2.124(5) 2.165 |
| \angle Cl1-Cr-Cl2 | 98.80(4) | 99.0(3) |
| \angle Cp-Py (angle between pyridyl [RMSD 0.016 Å] and Cp planes [RMSD 0.025 Å]) | 74.08(6) | 74.08(6) |

the organic ligand. While Cr1a (population 0.89) shows similar coordination geometry to the previously reported complexes of that type,^{6,7} Cr1b (population 0.11) is shifted toward the benzene moiety of indenyl. This is particularly evident in the distance Cr-C9, which is considerably shorter in **1a** compared to **1b** (respectively, 2.215(3) vs 2.534(6) Å, Table 1). These different positions of the chromium atoms lead to a small change in the distances to the nitrogen atom, whereas the internal geometry of the CrCl_2 moieties is quite similar. Hence, the two chromium atoms are in different local environments, whereas the intermolecular environment is quite similar for **1a** and **1b**. Therefore, an energy barrier between the two different binding modes in the solid state must be present, which leads to the appearance of the two structural isomers.

HFEPR. Complexes related to **1** were previously studied by HFEPR and exhibited good spectral response.⁸ Given this previous success, HFEPR experiments were performed on polycrystalline samples of **1** in the frequency range of 98–424 GHz and at $T = 10$ K. The samples were not ideal powders, though, as their sensitivity to air and humidity prevented thorough grinding. There was the additional concern that extreme grinding might affect the subtleties of crystal structure as described above. This affected the quality of the spectra, which, nevertheless, were fully interpretable.

The most important observation was that the spectra originated from two distinct spin species, both $S = 3/2$, i.e., corresponding to those expected from the $3d^3$ ion Cr(III) .⁸ This is illustrated in Figure 3, where we plotted the low-field region (0–2 T) of the spectra recorded using the 12th harmonic of the 12–14 GHz base source,⁹ and thus in the frequency range of 146–166 GHz. One can clearly see two

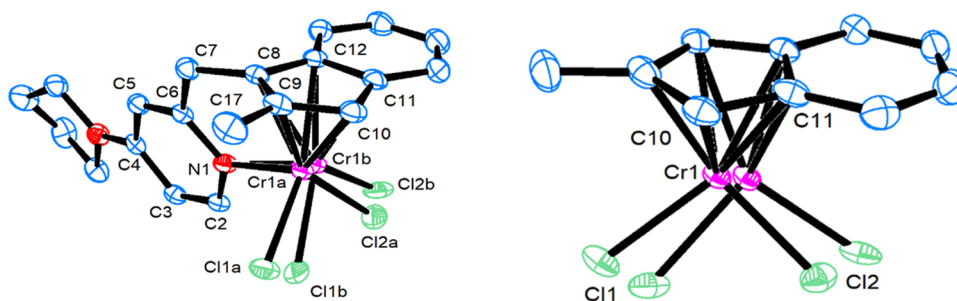


Figure 2. Left: Solid-state molecular structure of complex **1**. Blue: C, red: N, green: Cl, purple: Cr. H atoms are omitted for clarity. Displacement ellipsoids are drawn with 50% probability. For details of crystal structure analysis, see the [SI](#). Right: Another view of **1**. The pyridine substituent and H atoms are omitted. The labeled atoms Cl2-Cr1-C11-C10 represent the dihedral angle used for the potential energy surface scan (see below).

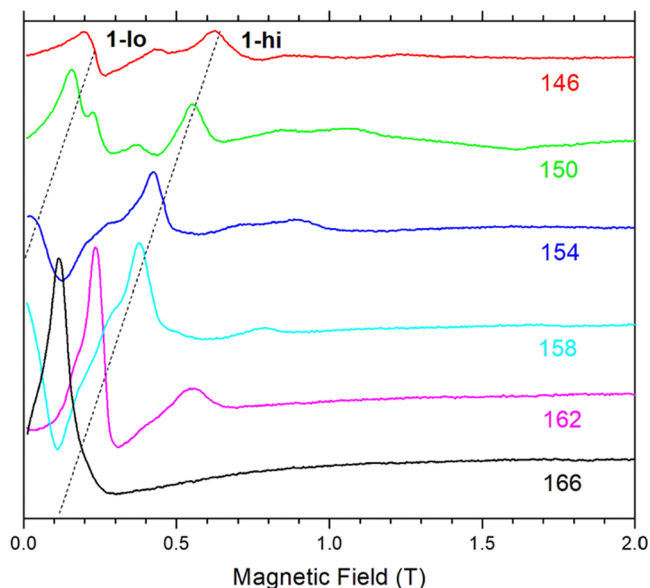


Figure 3. Low-field HFEPR spectra of polycrystalline complex **1** recorded at 10 K at the frequencies indicated in GHz. The dashed lines are a guide to the eye and point at the approximate frequencies of the zero-field resonances for species **1-lo** and **1-hi**, which for species **1-lo** is reached at about 156 GHz, but for **1-hi** is not reached until a frequency higher than 166 GHz.

resonances marked **1-hi** and **1-lo** that move to the lower field with increasing frequency.

One of them, **1-lo**, actually reaches zero field at about 156 GHz (5.2 cm^{-1}), while the other does not reach zero field even at the highest frequency, generated with this particular (12th) harmonic, 166 GHz. The position of that zero-field resonance can be estimated by interpolating the feature observed at 166 GHz and at the next higher available frequency, 202 GHz (not shown). This method gives the zero-field transition at ~ 180 GHz ($\sim 6 \text{ cm}^{-1}$). Since an $S = 3/2$ spin species can have only one zero-field energy gap, which is equal to $[2(D^2 + 3E^2)]^{1/2}$,¹ the obvious conclusion is that there are two distinct species in the sample, one characterized by $|D| \approx 3.0 \text{ cm}^{-1}$ (**1-hi**) and another by $|D| \approx 2.6 \text{ cm}^{-1}$ (**1-lo**), assuming for simplicity a fully axial zfs tensor ($E = 0$). The amplitude ratio of both species is about equal.

The zero-field resonances give an idea as to the axial zfs parameter D values for both spin species, but do not offer any values of the other spin Hamiltonian parameters. For this purpose, we performed HFEPR experiments in a two-dimensional space (magnetic field vs frequency) and plotted the corresponding map of observed turning points (Figure 4). Using the tunable-frequency methodology,³ we then fitted the five spin Hamiltonian parameters applicable for a fully rhombic $S = 3/2$ system, namely, D , E , g_x , g_y , and g_z , to this map, obtaining values as listed in Table 2. As expected and already shown in Figure 3, the two spin species (**1-hi** and **1-lo**) have different D -values (3.05 and 2.64 cm^{-1} , respectively). Determining the rhombic parameter E necessitated some assumptions since that parameter was obtained mostly from the intra-Kramers resonances within the $m_S = \pm 1/2$ doublet, which are not sensitive to the D -value, and consequently overlap for both spin species. We assumed that the species **1-hi** characterized by a larger D -value than species **1-lo**, has also a larger E -value. As an end result, the rhombicity factor E/D for species **1-hi** is about 0.06, while for species **1-lo**, about 0.03.

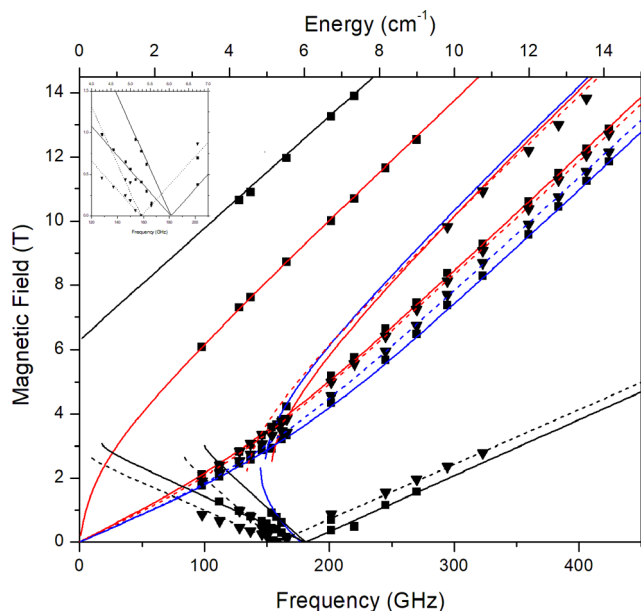


Figure 4. Field vs frequency (or energy) dependence of turning points in the HFEPR spectra of **1** at 10 K. The squares are experimental points attributed to species **1-hi**, while the triangles are those attributed to species **1-lo**. The curves are simulations using spin Hamiltonian parameters as in Table 2. Solid lines: species **1-hi**; dashed lines: species **1-lo**. Red lines: turning points with magnetic field, B_0 , parallel to the x -axis of the zfs tensor; blue: $B_0 || y$; black: $B_0 || z$. For clarity, only those turning points are plotted that are actually represented by identifiable experimental resonances. Inset: zoom-in view of the frequency region near the two zero-field transitions.

The g_x and g_y values came out from the fits as typical for the $3d^3$ configuration (i.e., $g < g_e$ (2.00) for less than half-filled d^n), just under 2.00, as seen previously for related organometallic complexes,⁸ and generally for Cr(III) coordination complexes,^{10–14} but the g_z value was slightly, but consistently larger than 2.00 for either species so that $g_{\text{avg}} = 1.997$. For comparison, Cr(acac)₃ doped into various diamagnetic hosts, M(acac)₃ M = Al, Co, Ga, gave $1.980 \leq g_{\text{iso}} \leq 1.997$, so the g_{avg} value seen here is not unusual.^{15,16} The g tensor anisotropy in Cr(III) coordination complexes is typically small or non-existent, but in other 3d ions with less than half-filled configurations, namely, $3d^4$ (Mn(III)^{17,18} and Fe(IV)^{19,20}), g value components as high as 2.08 have been reported.

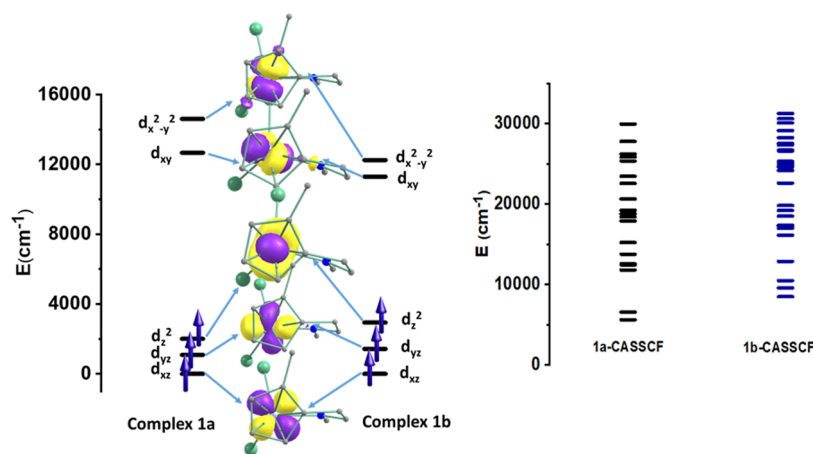
To determine the sign of D , simulating single-frequency spectra is indispensable. Figures S1 and S2 in the SI show such simulations for species **1-hi** and **1-lo**, respectively, near the high end of our frequencies, 385 GHz. Although simulations are not perfect due to the problems with sample crystallinity and possible torquing, they are quite satisfactory in that D is found positive for both species, consistent with our earlier results on related complexes.⁸ In particular, the low-temperature spectra are dominated in each species by the two perpendicular turning points of the intra-Kramers transition within the $m_S = \pm 1/2$ doublet (between 10 and 12 T) which must then be the ground state. In the case of $D < 0$, that doublet would be almost invisible, with the intra-Kramers transition within the $m_S = \pm 3/2$ doublet (which would be the ground-state doublet in this case) dominating (for species **1-lo**, between 13 and 14.5 T; for species **1-hi**, outside the field range).

Table 2. Experimental and Calculated Spin Hamiltonian Parameters (D and E in cm^{-1} and g Values) for **1** in Various Structural Forms

| complex ^a | experimental from HFEPR | | calculated by CASSCF | | calculated by NEVPT2 | | g-tensor EPR | | | g-tensor-CASSCF/NEVPT2 |
|-------------------------------------|-------------------------|----------------------|----------------------|-----------------|----------------------|---------------|--------------------------------------|----------|----------|--------------------------|
| | D | E (E/D) | D | E (E/D) | D | E (E/D) | g_{xx} | g_{yy} | g_{zz} | (g_{avg}) |
| 1a (1-hi) | 3.05(5) | 0.185(5), (0.061) | 3.20 | 0.65, (0.20) | 2.11 | 0.15 (0.07) | 1.94(2), 1.97(1), 2.08(2), (2.00) | | | 1.98, 1.99, 2.00, (1.99) |
| 1b (1-lo) | 2.64(5) | 0.088(5) (0.033) | 2.52 | 0.33, (0.13) | 2.36 | 0.28 (0.12) | 1.99(1), 1.98(1), 2.02(4), (2.00) | | | 1.95, 1.96, 1.98, (1.96) |
| 1 (solution) ^b | 2.85 | 0.14 (0.049) | | | | | 1.99, 1.99, 2.08, (2.02) | | | |
| 1 (DFT-optimized, gas phase) | | | 2.45 | 0.11 | 2.32 | 0.08 | | | | 1.96, 1.96, 1.99, (1.97) |

^aThe designations **1a** and **1b** refer to the two crystallographically identified structures (Figure 2), while the designations **1-hi** and **1-lo** refer to the two species identified by HFEPR (Figure 3). The calculations demonstrate the similarity of **1a** with **1-hi** and **1b** with **1-lo**, respectively.

^bDichloromethane-toluene 1:2 v/v.

**Figure 5.** ALLFT-calculated d-orbital splitting for complexes **1a** and **1b**. The orbital lobes of **1a** are shown on the left, and the corresponding energy levels of excited states derived through CASSCF are shown on the right.

Finally, we also performed HFEPR on a frozen solution of complex **1** in a 1:2 v/v mixture of dichloromethane and toluene. As usual, the solvent absorbed much of the incident sub-THz wave power, resulting in a decreased S/N ratio. Also, although the sample manipulation took place in a nominally air-free environment, a large part of the sample decomposed, resulting in a generic isotropic Cr(III) signal. Still, enough of the complex survived the procedure to yield spectra like the one shown in Figure S3 in the SI, recorded at 4.5 K and 166 GHz. These spectra show a presence of only one spin species, with the zfs parameters $D = 2.85$ and $E = 0.14 \text{ cm}^{-1}$, that is in between those of species **1-hi** and **1-lo** in the solid.

Quantum Chemical Theory (QCT) Calculations. QCT calculations used the ORCA 4.0/ORCA 4.0 software package.^{21,22} Two *ab initio* methods were used: complete-active space self-consistent field (CASSCF)^{23,24} followed by N electron valence second-order perturbation theory (NEVPT2)^{25–28} to take into account the dynamic correlation. Computational details are given in the Experimental Section. The experimental and theoretical spin Hamiltonian values are given in Table 2. To validate the experimentally determined zfs parameters from the EPR measurement, we have used the two molecular structures **1a** and **1b** as determined by XRD. Along with these, zfs parameters were calculated using a density functional theory (DFT) optimized structure of the complex as well (b3lyp/Cr-TZVP/C,N,Cl,H-6-311g(d,p)).

The calculated g tensor values obtained for different derivatives^{8,29} and different isomers are all very similar,

whereas zfs values vary more. The contrasting sensitivity of zfs and insensitivity of g values to electronic/geometrical structure in $S > 1/2$ systems is often seen experimentally by HFEPR and is discussed elsewhere.^{2,3,30,31} The current CASSCF results for both complexes (**1a** and **1b**, respectively) closely match the experimentally EPR-derived results (Table 2). The NEVPT2 result is slightly different for one of the geometries, as it takes the dynamic correlation into consideration and may be over-parameterizing the energy for **1a**. The calculated gas-phase result gives a zfs that is slightly smaller than that for **1b**, albeit not as directly in between **1a** and **1b** as the frozen solution result is. A gas-phase calculation is not the same as a structure in the mixed solvent system needed for EPR. Overall, the agreement between experimental and calculated zfs parameters is remarkable and agrees with the two structures seen crystallographically. The calculated g tensors are more anisotropic for **1b** than found experimentally for **1-lo** but are opposite for **1a** versus **1-hi**—more isotropic than found by HFEPR. Nevertheless, the discrepancy between calculated and experimental g values is trivial given that all g values of whatever provenance are in the range 2.01 ± 0.07 and, more importantly, the calculations reproduce the relationship $g_x \approx g_y < g_z$.

The differences in the zfs parameters between the two conformers are due to small structural changes leading to differences in the energy splitting of the five 3d orbitals of the Cr(III) center. The mechanism whereby the d orbital energy splitting gives rise to zfs via spin-orbit coupling (SOC) is

described in the SI with the use of both simple perturbation theory and ligand-field theory (LFT) calculations. The eigenvalue plot for the d orbital splitting obtained from the *ab initio* LFT (AILFT)³² approach is provided in Figure 5. The pattern of orbital splitting and the electron distribution remains the same for both complexes ($d_{xz}^1 d_{yz}^1 d_{z^2}^1 d_{xy}^0 d_{x^2-y^2}^0$) but the energy gaps among the corresponding orbitals is different. It is this different energy splitting between the two that is the origin of their different zfs as explained in the SI. The low-lying occupied orbitals for **1a** are close in energy (1089 and 2009 cm^{-1}) compared to **1b** (1429 and 2943 cm^{-1}), whereas the unoccupied orbitals in **1a** lie higher in energy compared to **1b**. This leads to a larger zfs for **1a** and a smaller zfs for **1b** as determined by QCT. The CASSCF transition energy levels for both complexes are shown in Figure 5. The CASSCF orbital energies for complex **1a** lie closely packed at a low level indicating more pronounced transitions among the low-lying states leading to the observation of a larger zfs than for **1b** where the levels are spaced slightly further apart in energy.

The *ab initio* QCT calculation above explains how a small change in structure can lead to significant changes in zfs parameters which can be detected by spectroscopic techniques. A ligand-field-based explanation for a difference in zfs could be the Cl-Cr-Cl bond angle (i.e., use of the angular overlap model (AOM)),³³ similar to what was seen in a Ti(II) complex.³⁴ However, this metric is essentially the same between the two forms making such a simple model insufficient. As mentioned above, the key metric in going from **1a** to **1b** is that the CrCl_2 moiety is shifted toward the benzene ring of indenyl. The Cr-C bond lengths become considerably different in **1b** so that only two out of five carbon atoms of the cyclopentadienide ring of indenyl are at a short distance to the metal atom. This η^2 -like coordination mode seems to be responsible for the lower zfs in **1b** (**1-lo**) as opposed to **1a** (**1-hi**). In solution, this double-well potential energy surface no longer exists and a species with an intermediate zfs and presumably an intermediate structure results.

Whereas XRD and EPR measurements demonstrated the existence of two structural isomers in the crystalline solid, only one species was detected by EPR in a frozen solution of complex **1**. We wanted to check if two structural isomers of the solid material may also exist in solution or in the gas phase. This is possible only if an energy barrier leading to a double-well potential separates them. DFT-based geometry optimizations were performed starting with the experimentally determined structures; however, they converge to a single minimum using standard optimization protocols without any geometry constraints. In cases where the potential energy landscape is very flat, geometry optimizations may overlook local minima with similar geometry. Therefore, we scanned different structures that resulted from constraining the dihedral angle Cl2-Cr1-C11-C10. This angle essentially captures the geometrical changes when going from structure **1a** to **1b** (see Figures 2 and 6) and thus $\angle\text{Cl2-Cr1-C11-C10}$ was incremented in steps of 2° from 105° to 155° . With this procedure, we identified two local minima at 120° and 133° as shown in Figure 6. However, further relaxed optimization of these two structures without any constraints led to a single global minimum with a dihedral angle of 128° . This value is close to the dihedral angle of one of the two isomers in the crystal (126.7° and 139.7°).

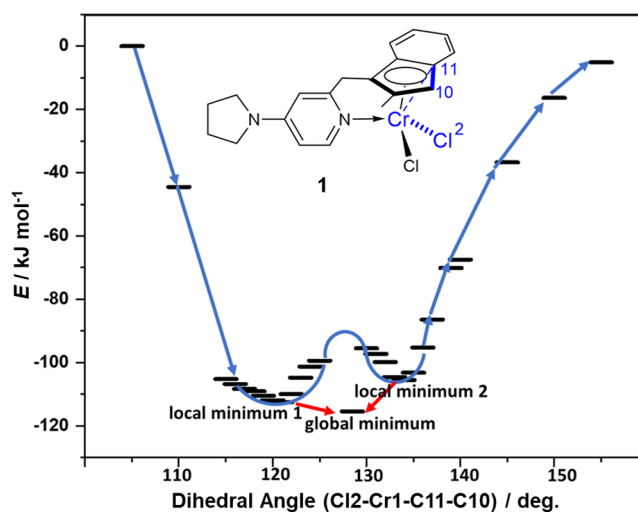


Figure 6. Potential energy surface scan along Cl2-Cr1-C11-C10 dihedral angle from 105° to 155° (blue curve and blue atoms in drawing of complex **1**). Local minima are at 120° and 133° , and a global minimum is at 128° that results from fully relaxed optimization. The results of each calculation are shown as black bars.

CONCLUSIONS

A catalytically relevant dichlorido organochromium(III) complex with an η^5 -indenyl ligand bearing a pendant pyridyl group, **1**, exhibits in solution, whether fluid by NMR, or frozen by EPR a single conformation. In contrast, in the solid state, the complex exhibits two conformations, **1a** and **1b**, that differ in the orientation of the CrCl_2 unit with respect to the indenyl ring. The HFEPR spectra of polycrystalline **1** show two species **1-hi** and **1-lo**, so named because the former has a larger axial zfs parameter, D , than the latter. These species can be correlated with the two conformations indicated by XRD. The amplitude ratio in EPR, which is about 1:1, can be correlated qualitatively only with the molar ratio that was found to be 0.89:0.11 in XRD. Quantum chemical theory calculations closely reproduce the two sets of parameters, correlating them with the two structures. The basis for these two distinct solid-state structures, as reflected in XRD and HFEPR and validated by theory, is unclear, but shows the conformational variability of such paramagnetic organometallic complexes, which may be related to their catalytic ability as well. That small structural differences seen in a precatalyst in the solid state lead to notable differences in electronic structure, as seen experimentally by HFEPR and validated by theory, suggests that active catalysts in solution may have slightly different conformations (e.g., from ring slippage) that are electronically distinct.

EXPERIMENTAL SECTION

Synthesis and Chemical Characterization. *Synthesis of Ligand.* To a solution of 2-methyl-4-(pyrrolidin-1-yl)pyridine (1.70 g, 10.5 mmol, 1.00 equiv) in thf (20 mL) cooled to -20°C was added a 2.5 M solution of *n*-BuLi in hexane (4.40 mL, 11.0 mmol, 1.05 equiv) over 20 min. After warming up to rt, 2-methyl-1-indanone (1.53 g, 10.5 mmol, 1.00 equiv) was added and the resulting mixture was stirred for 1 h. Subsequently, the reaction was acidified with conc. HCl (6 mL) and stirred for another 30 min at rt. Then, the solution was made basic with aqueous ammonia and the layers were separated. The aqueous layer was extracted with CH_2Cl_2 (3×20 mL), the combined organic layers were dried over MgSO_4 , and the solvent was removed under reduced pressure. Column chromatography (silica,

EE/PE/TEA = 30:10:1, $R_f = 0.31$) yielded the target compound as a colorless solid (2.30 g, 7.92 mmol, 76%).

¹H NMR (600 MHz, CDCl₃): δ [ppm] = 1.97 (m, 4H, CH₂), 2.17 (s, 3H, CH₃), 3.16 (m, 4H, CH₂), 3.37 (s, 2H, CH₂), 3.96 (s, 2H, CH₂), 6.15 (m, $J = 2.4$ Hz, 1H, CH), 6.21 (m, $J = 5.9$ Hz, 2.4 Hz, 1H, CH), 7.07 (m, $J = 7.4$ Hz, 1.0 Hz, 1H, CH), 7.17 (m, $J = 7.4$ Hz, 1H, CH), 7.23 (m, $J = 7.4$ Hz, 1H, CH), 7.36 (m, $J = 7.4$ Hz, 1H, CH), 8.15 (m, $J = 5.9$ Hz, 1H, CH).

Synthesis of Complex 1. The ligand (607 mg, 2.09 mmol, 1.00 equiv) was dissolved in thf (16 mL), and potassium hydride (88.0 mg, 2.19 mmol, 1.05 equiv) was added. Effervescence could be observed, and the resulting red suspension was stirred at room temperature for 18 h. Solid CrCl₃(thf)₃ (783 mg, 2.09 mmol, 1.00 equiv) was added producing a dark green solution that was stirred for 2 h. A turquoise precipitate was formed and separated from the solution with a centrifuge. The residue was washed with thf (4 × 4 mL) and pentane (2 × 5 mL). A solution of the turquoise residue in CH₂Cl₂ was filtered over celite to remove KCl and then recrystallized by diffusion of pentane into the solution. Complex 1 (421 mg, 1.02 mmol, 48%) was obtained as dark green crystals.

¹H NMR (600 MHz, CD₂Cl₂): δ [ppm] = -111.4, -20.0, -12.8, -11.1, 1.87, 30.5, 37.7, 40.1, 43.68, 48.7, 55.6. LIFDI-MS (m/z [rel. int.]): calc.: 411.1, fnd.: 411.1 [100]

EA: C₂₀H₂₁Cl₂CrN₂: calc. (found): C: 58.26 (57.65); H: 5.13 (5.05); N: 6.79 (6.85).

XRD. Crystallography of 1 was performed at 120 K with a Mo K α , 0.71073 Å X-ray source. The space group of complex 1 is P2₁/n with a monoclinic crystal system. Details of the crystal structure determination are compiled in the Supporting Information.

HFEPR. HFEPR spectra were recorded using a 15/17 T magnet-based spectrometer described previously,⁹ except that solid-state sources (Virginia Diodes, Charlottesville, VA) operating at 12–14 GHz were used in conjunction with a cascade of multipliers (through the 32nd harmonic). The sample size was typically 40 mg. Spectral simulations used the program SPIN (A. Ozarowski, NHMFL) with a standard spin Hamiltonian for $S = 3/2$

$$H = \beta_e \cdot g \cdot \hat{S} + D \left[\hat{S}_z^2 - \frac{S(S+1)}{3} \right] + E [\hat{S}_x^2 - \hat{S}_y^2]$$

where β_e is the Bohr magneton, g is the spectroscopic, g is the tensor, and D and E are axial and rhombic, respectively, second-order zero-field splitting (zfs) parameters. Higher-order terms are not applicable for $S = 3/2$.

QCT. All calculations were performed using the ORCA 4.0 package.^{21,22} State averaged complete-active space self-consistent field (SA-CASSCF) wave functions were computed first followed by N -electron valence second-order perturbation theory (NEVPT2) for taking into account the role of dynamic correlation. For the CASSCF calculations, we have included three Cr electrons in 5 d orbitals as the active space [CAS(3,5)]. The active space spans 10 quartet states and 40 doublet states for complex 1, which is the entire d³ configuration. The polarized triple- ζ quality of the Douglas–Kroll–Hess (DKH)³⁵-type basis set [DKH-def2-TZVP]³⁶ was used for Cr, DKH-def2-TZVP(-f) for N and Cl; and DKH-def2-SVP was used for C and H atoms. To speed up the calculations, we have implemented the TrafoStep RIMO approximation for CASSCF and RI-approximation for NEVPT2. The spin-orbit coupling was taken into account through the Quasi-Degenerate Perturbation Theory (QDPT) approach, and for the zfs (D) and g tensors, the effective Hamiltonian approach was employed.³⁷

■ ASSOCIATED CONTENT

Supporting Information

The Supporting Information is available free of charge at <https://pubs.acs.org/doi/10.1021/acs.organomet.2c00182>.

Additional HFEPR spectra and simulations, NMR spectrum, details of X-ray crystal structure determi-

nation, ligand-field theory (LFT) analysis, and quantum chemical theory (QCT) methods (PDF)

Accession Codes

CCDC 2155444 contains the supplementary crystallographic data for this paper. These data can be obtained free of charge via www.ccdc.cam.ac.uk/data_request/cif, or by emailing data_request@ccdc.cam.ac.uk, or by contacting The Cambridge Crystallographic Data Centre, 12 Union Road, Cambridge CB2 1EZ, UK; fax: +44 1223 336033.

■ AUTHOR INFORMATION

Corresponding Authors

Joshua Telser – Department of Biological, Physical, and Health Sciences, Roosevelt University, Chicago, Illinois 60605, United States; orcid.org/0000-0003-3307-2556; Email: jtels@roosevelt.edu

Markus Enders – Institute of Inorganic Chemistry, Heidelberg University, 69120 Heidelberg, Germany; orcid.org/0000-0003-0415-1992; Email: markus.enders@uni-heidelberg.de

Authors

Helge-Boj Hansen – Institute of Inorganic Chemistry, Heidelberg University, 69120 Heidelberg, Germany

J. Krzystek – National High Magnetic Field Laboratory, Florida State University, Tallahassee, Florida 32310, United States; orcid.org/0000-0001-6088-1936

Abinash Swain – Institute of Inorganic Chemistry, Heidelberg University, 69120 Heidelberg, Germany; Department of Chemistry, Indian Institute of Technology Bombay, Mumbai 400076, India

Gopalan Rajaraman – Department of Chemistry, Indian Institute of Technology Bombay, Mumbai 400076, India

Hubert Wadepohl – Institute of Inorganic Chemistry, Heidelberg University, 69120 Heidelberg, Germany

Complete contact information is available at:

<https://pubs.acs.org/10.1021/acs.organomet.2c00182>

Notes

The authors declare no competing financial interest.

■ ACKNOWLEDGMENTS

Part of this work was performed at the National High Magnetic Field Laboratory (NHMFL), funded by National Science Foundation through Cooperative Agreement 1644779 and the State of Florida. The authors thank the state of Baden-Württemberg through bwHPC and the German Research Foundation (DFG) through grant no. INST 40/467-1 FUGG (JUSTUS cluster). They also thank Dr. Andrew Ozarowski (NHMFL) for use of the EPR simulation software SPIN.

■ REFERENCES

- Schweinfurth, D.; Krzystek, J.; Atanasov, M.; Klein, J.; Hohloch, S.; Telser, J.; Demeshko, S.; Meyer, F.; Neese, F.; Sarkar, B. Tuning Magnetic Anisotropy Through Ligand Substitution in Five-Coordinate Co(II) Complexes. *Inorg. Chem.* **2017**, *56*, 5253–5265.
- Krzystek, J.; Telser, J. Measuring giant anisotropy in paramagnetic transition metal complexes with relevance to single-ion magnetism. *Dalton Trans.* **2016**, *45*, 16751–16763.
- Krzystek, J.; Ozarowski, A.; Telser, J. Multi-frequency, high-field EPR as a powerful tool to accurately determine zero-field splitting in high-spin transition metal coordination complexes. *Coord. Chem. Rev.* **2006**, *250*, 2308–2324.

- (4) O'Connor, J. M.; Casey, C. P. Ring-slippage chemistry of transition metal cyclopentadienyl and indenyl complexes. *Chem. Rev.* **1987**, *87*, 307–318.
- (5) Calhorda, M. J.; Romão, C. C.; Veiros, L. F. The Nature of the Indenyl Effect. *Chem.-Eur. J.* **2002**, *8*, 868–875.
- (6) Hansen, H.-B.; Wade, H.; Enders, M. The Stronger the Better: Donor Substituents Push Catalytic Activity of Molecular Chromium Olefin Polymerization Catalysts. *Chem.-Eur. J.* **2021**, *27*, 11084–11093.
- (7) Hansen, H.-B.; Wade, H.; Enders, M. Improved Single-Site Chromium Catalysts with Electron Rich Indenyl Ligands for the Formation of Ultrahigh Molecular Weight Polyethylene. *Eur. J. Inorg. Chem.* **2021**, *2021*, 1278–1286.
- (8) Krzystek, J.; Kohl, G.; Hansen, H.-B.; Enders, M.; Telser, J. Combining HFEP and NMR Spectroscopies to Characterize Organochromium(III) Complexes with Large Zero-Field Splitting. *Organometallics* **2019**, *38*, 2179–2188.
- (9) Hassan, A. K.; Pardi, L. A.; Krzystek, J.; Sienkiewicz, A.; Goy, P.; Rohrer, M.; Brunel, L. C. Ultrawide Band Multifrequency High-Field EMR Technique: A Methodology for Increasing Spectroscopic Information. *J. Magn. Reson.* **2000**, *142*, 300–312.
- (10) Pedersen, E.; Toftlund, H. Electron spin resonance spectra of tetragonal chromium(III) complexes. I. *trans*-[Cr(NH₃)₄XY]ⁿ⁺ and *trans*-Cr(py)₄XY]ⁿ⁺ in frozen solutions and powders. Correlation between zero-field splittings and ligand field parameters via complete d-electron calculations. *Inorg. Chem.* **1974**, *13*, 1603–1612.
- (11) McGarvey, B. R. Spin Hamiltonian for Cr III Complexes. Calculation from Crystal Field and Molecular Orbital Models and ESR Determination for Some Ethylenediamine Complexes. *J. Chem. Phys.* **1964**, *41*, 3743–3758.
- (12) Hempel, J. C.; Morgan, L. O.; Lewis, W. B. Electron paramagnetic resonance of *trans*-disubstituted bis(ethylenediamine)-chromium(III) complexes in frozen solutions. *Inorg. Chem.* **1970**, *9*, 2064–2072.
- (13) Solano-Peralta, A.; Sosa-Torres, M. E.; Flores-Alamo, M.; El-Mkami, H.; Smith, G. M.; Toscano, R. A.; Nakamura, T. High-field EPR study and crystal and molecular structure of *trans*-RSSR-[CrCl₂(cyclam)]_nX (X = ZnCl₄²⁻, Cl⁻ and Cl⁻·4H₂O·0.5HCl). *Dalton Trans.* **2004**, 2444–2449.
- (14) Campanella, A. J.; Nguyen, M.-T.; Zhang, J.; Ngendahimana, T.; Antholine, W. E.; Eaton, G. R.; Eaton, S. S.; Glezakou, V.-A.; Zadrozny, J. M. Ligand control of low-frequency electron paramagnetic resonance linewidth in Cr(III) complexes. *Dalton Trans.* **2021**, *50*, 5342–5350.
- (15) McGarvey, B. R. Anisotropic Hyperfine Interaction of Cr⁵³ in Chromium (III) Acetylacetonate. *J. Chem. Phys.* **1964**, *40*, 809–812.
- (16) Elbers, G.; Remme, S.; Lehmann, G. EPR of Cr³⁺ in tris(acetylacetonato)gallium(III) single crystals. *Inorg. Chem.* **1986**, *25*, 896–897.
- (17) Sunatsuki, Y.; Kishima, Y.; Kobayashi, T.; Yamaguchi, T.; Suzuki, T.; Kojima, M.; Krzystek, J.; Sundberg, M. R. A single tripodal ligand stabilizing three different oxidation states (II, III, and IV) of manganese. *Chem. Commun.* **2011**, *47*, 9149–9151.
- (18) Romain, S.; Duboc, C.; Neese, F.; Rivière, E.; Hanton, L. R.; Blackman, A. G.; Philouze, C.; Leprêtre, J.-C.; Deronzier, A.; Collomb, M.-N. An Unusual Stable Mononuclear Mn^{III} Bis-terpyridine Complex Exhibiting Jahn–Teller Compression: Electrochemical Synthesis, Physical Characterisation and Theoretical Study. *Chem.-Eur. J.* **2009**, *15*, 980–988.
- (19) Rasheed, W.; Draksharapu, A.; Banerjee, S.; Young, V. G., Jr.; Fan, R.; Guo, Y.; Ozerov, M.; Nehr Korn, J.; Krzystek, J.; Telser, J.; Que, L., Jr. Crystallographic Evidence for a Sterically Induced Ferryl Tilt in a Non-Heme Oxidation(IV) Complex that Makes it a Better Oxidant. *Angew. Chem., Int. Ed.* **2018**, *57*, 9387–9391.
- (20) Bucinsky, L.; Rohde, G. T.; Que, L.; Ozarowski, A.; Krzystek, J.; Breza, M.; Telser, J. HFEP and Computational Studies on the Electronic Structure of a High-Spin Oxidation(IV) Complex in Solution. *Inorg. Chem.* **2016**, *55*, 3933–3945.
- (21) Neese, F. The ORCA program system. *WIREs Comput. Mol. Sci.* **2012**, *2*, 73–78.
- (22) Neese, F. Software update: The ORCA program system, version 4.0. *WIREs Comput. Mol. Sci.* **2018**, *8*, No. e1327.
- (23) Malmqvist, P.-Å.; Roos, B. O. The CASSCF state interaction method. *Chem. Phys. Lett.* **1989**, *155*, 189–194.
- (24) Olsen, J. The CASSCF method: A perspective and commentary. *Int. J. Quantum Chem.* **2011**, *111*, 3267–3272.
- (25) Angeli, C.; Cimiraglia, R.; Evangelisti, S.; Leininger, T.; Malrieu, J.-P. Introduction of *n*-electron valence states for multi-reference perturbation theory. *J. Chem. Phys.* **2001**, *114*, 10252–10264.
- (26) Angeli, C.; Cimiraglia, R.; Malrieu, J.-P. *N*-electron valence state perturbation theory: a fast implementation of the strongly contracted variant. *Chem. Phys. Lett.* **2001**, *350*, 297–305.
- (27) Angeli, C.; Cimiraglia, R.; Malrieu, J.-P. *n*-electron valence state perturbation theory: A spinless formulation and an efficient implementation of the strongly contracted and of the partially contracted variants. *J. Chem. Phys.* **2002**, *117*, 9138–9153.
- (28) Angeli, C.; Borini, S.; Cimiraglia, R. An application of second-order *n*-electron valence state perturbation theory to the calculation of excited states. *Theor. Chem. Acc.* **2004**, *111*, 352–357.
- (29) Rouf, S. A.; Mares, J.; Vaara, J. Relativistic Approximations to Paramagnetic NMR Chemical Shift and Shielding Anisotropy in Transition Metal Systems. *J. Chem. Theory Comput.* **2017**, *13*, 3731–3745.
- (30) Zolnhofer, E. M.; Opalade, A. A.; Jackson, T. A.; Heinemann, F. W.; Meyer, K.; Krzystek, J.; Ozarowski, A.; Telser, J. Electronic Structure and Magnetic Properties of a Low-Spin Cr^{II} Complex: *trans*-[CrCl₂(dmpe)₂] (dmpe = 1,2-Bis(dimethylphosphino)ethane). *Inorg. Chem.* **2021**, *60*, 17865–17877.
- (31) Telser, J.; Krzystek, J.; Ozarowski, A. High-frequency and high-field electron paramagnetic resonance (HFEP): a new spectroscopic tool for bioinorganic chemistry. *JBIC, J. Biol. Inorg. Chem.* **2014**, *19*, 297–318.
- (32) Singh, S. K.; Eng, J.; Atanasov, M.; Neese, F. Covalency and chemical bonding in transition metal complexes: An ab initio based ligand field perspective. *Coord. Chem. Rev.* **2017**, *344*, 2–25.
- (33) Bendix, J. 2.55 - Ligfield. In *Comprehensive Coordination Chemistry II*, McCleverty, J. A.; Meyer, T. J., Eds.; Pergamon: Oxford, 2003; pp 673–676.
- (34) Reinholdt, A.; Pividori, D.; Laughlin, A. L.; DiMucci, I. M.; MacMillan, S. N.; Jafari, M. G.; Gau, M. R.; Carroll, P. J.; Krzystek, J.; Ozarowski, A.; Telser, J.; Lancaster, K. M.; Meyer, K.; Mindiola, D. J. A Mononuclear and High-Spin Tetrahedral Ti^{II} Complex. *Inorg. Chem.* **2020**, *59*, 17834–17850.
- (35) Douglas, M.; Kroll, N. M. Quantum electrodynamic corrections to the fine structure of helium. *Ann. Phys.* **1974**, *82*, 89–155.
- (36) Pantazis, D. A.; Chen, X.-Y.; Landis, C. R.; Neese, F. All-electron scalar relativistic basis sets for third-row transition metal atoms. *J. Chem. Theory Comput.* **2008**, *4*, 908–919.
- (37) Maurice, R.; Bastardis, R.; de Graaf, C.; Suaud, N.; Mallah, T.; Guihéry, N. Universal Theoretical Approach to Extract Anisotropic Spin Hamiltonians. *J. Chem. Theory Comput.* **2009**, *5*, 2977–2984.